ADVANCED MATERIALS
www.advmat.de

Controlling the Emission Zone by Additives for Improved Light-Emitting Electrochemical Cells

*Joan Ràfols-Ribé, Xiaoying Zhang, Christian Larsen, Petter Lundberg, E. Mattias Lindh, Cuc Thu Mai, Jonas Mindemark, Eduardo Gracia-Espino, and Ludvig Edman**

The position of the emission zone (EZ) in the active material of a light-emitting electrochemical cell (LEC) has a profound influence on its performance because of microcavity effects and doping- and electrode-induced quenching. Previous attempts of EZ control have focused on the two principal constituents in the active material—the organic semiconductor (OSC) and the mobile ions—but this study demonstrates that it is possible to effectively control the EZ position through the inclusion of an appropriate additive into the active material. More specifically, it is shown that a mere modification of the end group on an added neutral compound, which also functions as an ion transporter, results in a shifted EZ from close to the anode to the center of the active material, which translates into a 60% improvement of the power efficiency. This particular finding is rationalized by a lowering of the effective electron mobility of the OSC through specific additive: OSC interactions, but the more important generic conclusion is that it is possible to control the EZ position, and thereby the LEC performance, by the straightforward inclusion of an easily tuned additive in the active material.

1. Introduction

The light-emitting electrochemical cell (LEC)[1] and the organic light-emitting diode (OLED)[2] are emerging electroluminescent (EL) technologies, which essentially comprise a thin active material sandwiched between a reflective electrode and a transparent electrode. This thin-film device architecture is attractive since it enables a number of exciting architectural opportunities, including glare-free and diffuse areal emission and lightweight and conformable luminaries. However, the characteristic thin and planar device structure also brings several challenges, notably related to that the photons generated within the sub-micrometer thin active material are highly sensitive to microcavity effects[3] and electrode- and doping-induced quenching.[4]

The good news is that these problems can be alleviated by a careful and rational design of the photon-generating emission zone (EZ) within the active material. In OLEDs, this is commonly effectuated by the division of the thin active material into a multitude of even thinner sublayers, with one such appropriately positioned and designed sublayer performing the task of the EZ whereas the other sublayers assist with the injection and the transport of the electronic charge carriers.[3,5] The drawback is that this type of nm-precise (and air-sensitive) multi-layer structure commonly requires expensive fabrication by thermal evaporation under high-vacuum conditions.

The LEC is distinguished from the OLED by the inclusion of mobile ions into the active material, where they are blended with an EL organic semiconductor (OSC). The mobile ions play a critical role during the initial LEC operation. In brief, when a voltage is applied, the mobile ions redistribute to first form injection-facilitating electrical double layers (EDLs) at the electrode interfaces, and thereafter enable for electrochemical p- and n-type doping of the OSC. These doping regions meet in the active material under the formation of a p-n junction, which essentially defines the EZ position.[6] This in situ formation of a "multilayer" structure in LEC devices is attractive since it enables for their low-cost printing and coating fabrication,[7] but is also challenging since it renders the control of the EZ less intuitive and difficult.[1d,6a,8]

It is thus motivated to develop and establish understanding and guidelines for the control of the EZ (and the doping structure) in LEC devices. Up to now, the primary tool for the control of the EZ in LECs has been through the selection of the OSC. More specifically, by employing a combination of different OSCs it has been shown possible to tune the position and/or the width of the EZ,[9] while the fabrication of a

J. Ràfols-Ribé, X. Zhang, C. Larsen, P. Lundberg, E. Gracia-Espino, L. Edman
The Organic Photonics and Electronics Group
Umeå University
Umeå SE-90187, Sweden
E-mail: ludvig.edman@umu.se
C. Larsen, L. Edman
LunaLEC AB
Umeå University
Umeå SE-90187, Sweden
E. M. Lindh
RISE Energy Technology Center AB
Industrigatan 1, Piteå SE-941 38, Sweden
C. T. Mai, J. Mindemark
Department of Chemistry – Ångström Laboratory
Uppsala University
Uppsala SE-751 21, Sweden
The ORCID identification number(s) for the author(s) of this article can be found under https://doi.org/10.1002/adma.202107849.

DOI: 10.1002/adma.202107849

solution-processed OSC multilayer structure can allow for a pinning of the EZ at an interface between two neighboring OSC layers.[9b,10] It has also proven possible to control the EZ through the selection and concentration of the mobile ions. Hu and co-workers,[11] and later Shin et al.,[12] demonstrated that the initial EZ position in open LEC devices, with extremely large interelectrode gaps of 1 mm or more, is affected by the selection of the salt cation, while Sun and co-workers[13] used a set of ionic liquids with a differently sized imidazolium cation for the control of the EZ position in conventional sandwich-cell LECs. Finally, Fang and co-workers showed that the selected value for the ion concentration in the active material controls the steady-state doping concentration and thereby the effective width of the EZ.[14]

Here, we report that the position of the EZ in LEC devices can be controlled for improved performance through the addition of a third non-essential component to the active material. Specifically, we have investigated two different star-shaped ion-transporter molecules for this additive, which are solely distinguished by their end-capping unit, which is either polar and short or more hydrophobic and extended. The addition of the latter results in a steady-state EZ located close to the anode, while the inclusion of the former shifts the steady-state EZ position to the center of the active material. A combination of the two ion transporters does, as expected, result in an intermediate EZ position. For the investigated devices, this shift of the EZ position from close to the anode to the center of the active material is manifested in an improvement of the power efficiency for light emission by 60% and through the attainment of an angle-independent luminance. We rationalize our findings by simulations and additional experiments, which suggest that the centering of the EZ is accomplished through a lowering of the effective electron mobility of the OSC following the inclusion of the more polar ion-transporter additive. An important take-home message of our study is, thus, that it is possible to control the EZ position for the desired LEC performance by the straightforward inclusion of an easily tuned, and potentially low-cost, additive.

2. Results and Discussion

We have fabricated and characterized three principal types of LEC devices with an active material comprising the conjugated polymer Super Yellow as the electroluminescent OSC and the salt KCF_3SO_3 dissolved in an ion transporter as the electrolyte, sandwiched between a reflective Al cathode and a transparent indium tin oxide (ITO) anode on a glass substrate. The different LECs are solely distinguished by the selection of the ion-transporter additive, which is a branched trimethylolpropane ethoxylate (TMPE) oligomer that is end-capped with either three short and hydrophilic hydroxyl groups (TMPE-OH) or three longer and more hydrophobic octyl carbonate groups (TMPE-OC). **Figure 1**a displays the chemical structure of the constituents in the active material, while Figure 1b is a schematic of the LEC device architecture. The latter also identifies the thickness of the active material layer as d_{AM} and the normalized position of the EZ in the active material, with the ITO/active-material interface located at 0 and the Al/active-material interface at 1. Figure 1c is a schematic of the spectrogoniometer setup, which

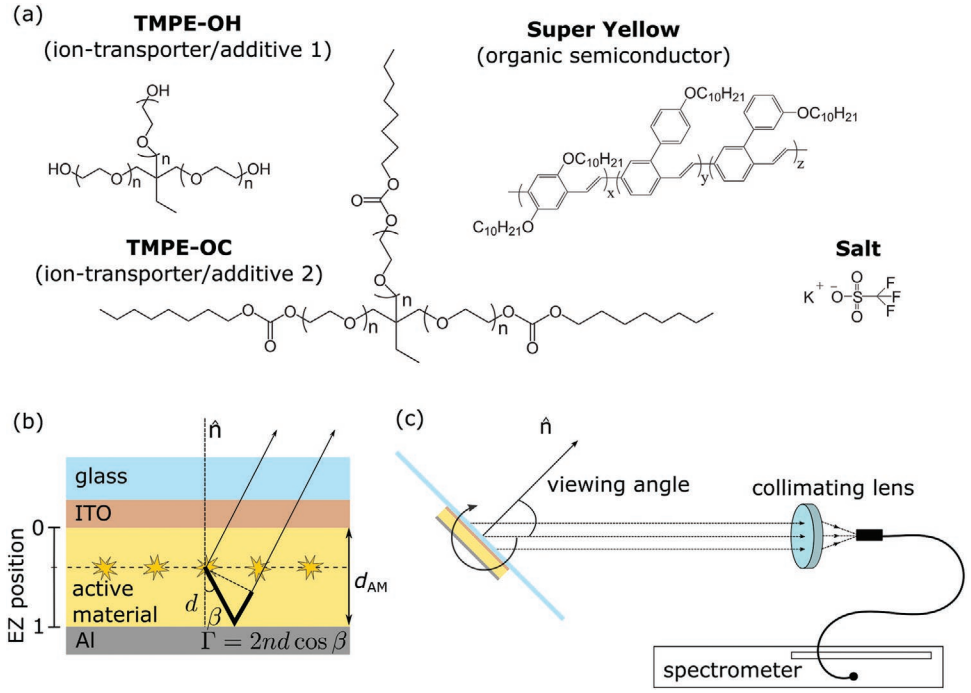

Figure 1. a) The chemical structure of the constituents in the LEC active material, including the distinguishing ion-transporter additives: TMPE-OH and TMPE-OC. b) A schematic of the LEC device architecture, which defines the thickness of the active material, d_{AM}, the position of the emission zone (EZ) in the active material, and the optical path difference Γ (marked by the thick black line) and its determining parameters. c) A schematic of the spectrogoniometer setup that measures the angle-dependent emission spectra and intensity.

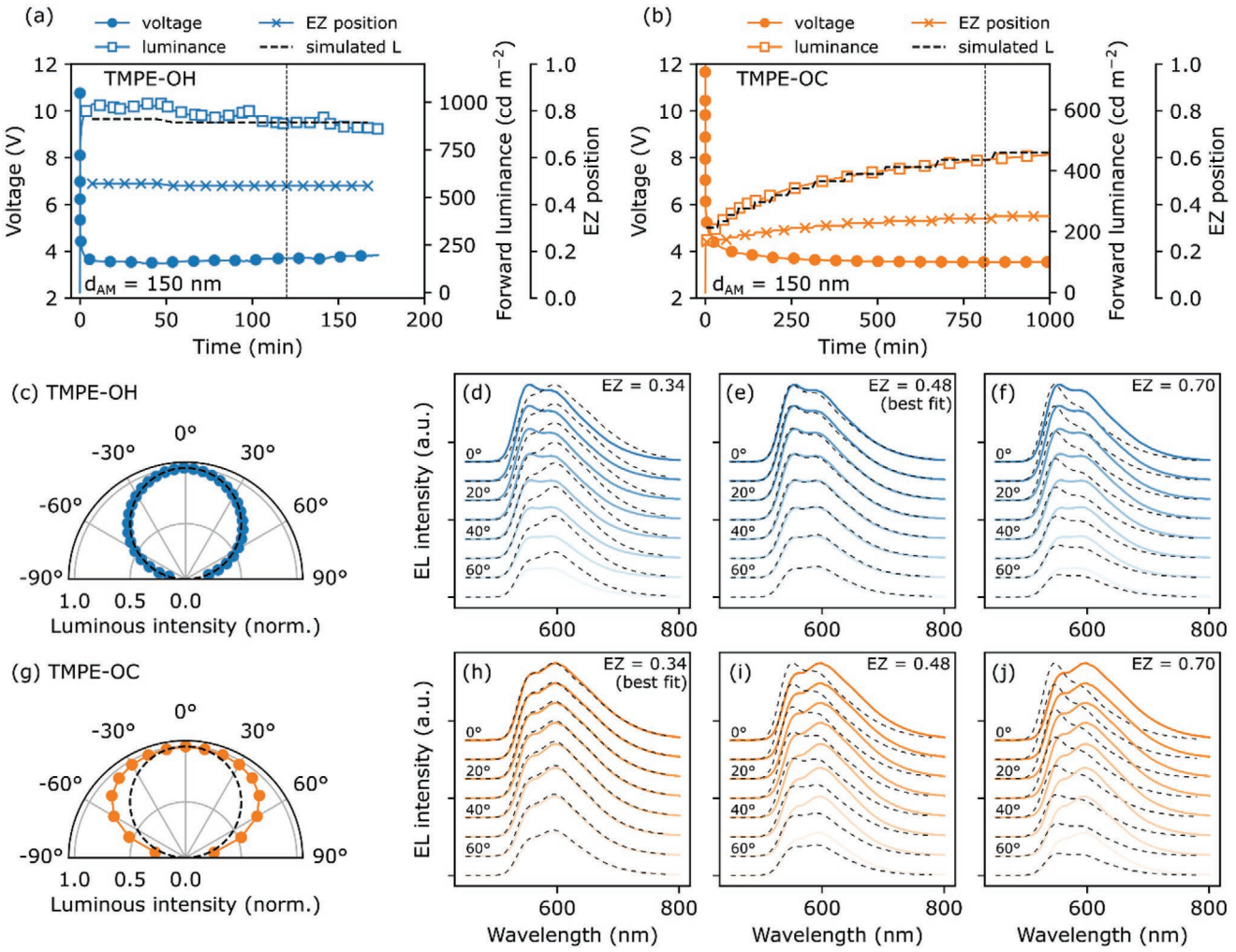

Figure 2. The temporal evolution of the voltage (filled circles), the measured forward luminance (open squares), the simulated forward luminance (dashed line), and the position of the EZ (crosses) for LEC devices with the ion transporter being: a) TMPE-OH, b) TMPE-OC. The active-material thickness is 150 nm, and the vertical dotted line indicates the time at which a stable steady-state performance is obtained. The anodic interface is located at 0 and the cathodic interface at 1. c,g) A polar plot of the normalized measured luminous intensity as a function of viewing angle at steady state.The dashed line represents the behavior of a Lambertian emitter. d–f,h–j) The measured (solid lines) and the simulated (dashed lines) EL spectra at steady state for a set of viewing angles (between 0° and 70°). The position of the EZ was varied in the simulations, as identified in the upper right corner of the graphs.

measures the angle-dependence of the EL spectrum and the EL intensity. More details on the LEC fabrication and the measurement procedures can be found in the Experimental Section.

Figure 2a,b presents the time evolution for the voltage (filled circles), the forward luminance (open squares), and the EZ position (crosses) for the TMPE-OH LEC (Figure 2a) and the TMPE-OC LEC (Figure 2b). The LECs were driven by a constant current density of 25 mA cm^{-2}, and d_{AM} was 150 nm. Figure S1, Supporting Information, presents the corresponding transients for an LEC with a blend of TMPE-OH and TMPE-OC as the ion transporter (in a 1:1 mass ratio) with the same active-material thickness, while Figure S2, Supporting Information, presents the corresponding transients for a set of TMPE-OH LECs with d_{AM} ranging between 117 and 376 nm. The position of the EZ in the active material was determined by first measuring the angle-dependent EL spectra (with the setup presented in Figure 1c), thereafter simulating the angle-dependent EL spectra as a function of the EZ position, and finally identifying which EZ position value in the simulation that provided the best agreement with the measured data. Two examples of this fitting procedure are visualized in Figure 2d–f,h–j, which yield that the best fit (at steady state) is provided with an EZ position of 0.48 for the TMPE-OH LEC and 0.34 for the TMPE-OC LEC. More details on the simulation and fitting procedures are presented in the Experimental Section.

We mention that a higher emission efficiency has been attained for similar LECs, but that these devices were separately optimized as regards to salt selection and concentration, d_{AM}, processing solvent, and driving protocol.[8b,15] However, since our aim here is to provide a direct and easy-to-interpret comparison of the effects of the different ion-transporter additives on the device performance, we have opted for a compromise in the form of a common and straightforward fabrication and driving protocol. In this context, it is relevant that the relative

position of the EZ in the inter-electrode gap is found to be essentially independent on d_{AM}, as displayed in Figure S2, Supporting Information, and as reported in refs. [4c,16]. We further mention that we have tested 4–8 independent devices for each ion-transporter selection and active-material thickness and that the device performance is highly repeatable. The presented results in Figure 2, Figures S1,S2, Supporting Information, and as summarized in Table S1, Supporting Information, are for the average device in each category.

All investigated LEC devices exhibit a decreasing voltage (solid circles) during the initial constant-current operation. This is a characteristic feature of a functional LEC, which signals the formation of EDLs (for improved electron/hole injection) and the subsequent formation of a light-emitting p-n junction by electrochemical doping (for improved electron and hole transport).[17] Figure 2a,b further shows that the two LECs feature a similar minimum voltage (V_{min}) of 3.5 V, which indicates a similar level of doping at steady state. This is rationalized by that both devices feature the same ion concentration (and d_{AM}), and that the initial ion concentration is dictating the average doping concentration at steady state.[14,18] In contrast, the time to V_{min} (at the same d_{AM}) is significantly shorter with TMPE-OH than TMPE-OC as the ion transporter. Similarly, the time to steady state at which also the luminance and the EZ position have stabilized (since the net motion of ions is zero)[19] is also shorter for the TMPE-OH LEC. This suggests that the total ion mobility in the active material is higher with the smaller TMPE-OH as the ion-transporter additive than the larger TMPE-OC.

Importantly, Figure 2 and Figure S1, Supporting Information, further reveal that the light-emission properties are strongly dependent on the selection of the ion-transporter additive. Specifically, we find that the TMPE-OH LEC (with d_{AM} = 150 nm) exhibits a >100% higher forward luminance and a 60% higher power efficacy than the TMPE-OC LEC (Figure 2a,b). The TMPE-OH LEC further delivers an emission intensity that is essentially independent of the viewing angle (as an ideal Lambertian emitter),[20] whereas the TMPE-OC LEC instead delivers its strongest emission intensity at larger viewing angles (Figure 2c,g). Moreover, the forward EL spectrum is also distinctly different, with the spectral envelope of the TMPE-OC LEC being redshifted with respect to that of the TMPE-OH LEC (compare solid lines in Figure 2d,h). We also find that both the transient and the steady-state behavior of the EZ position differ between the two LECs. For the TMPE-OH LEC (Figure 2a; Figure S2, Supporting Information), the EZ first forms closer to the cathode, and thereafter shifts to the center of the active material to stabilize at ≈0.48 at steady state (note that this transient is easier to distinguish for the slower devices with d_{AM} >150 nm in Figure S2, Supporting Information). This is in strong contrast to the situation for the TMPE-OC LEC (Figure 2b), for which the EZ first forms close to the anode at ≈0.24 and then shifts to reach ≈0.34 at steady state. We note that a similar transient shift of the EZ during LEC operation has been reported for several different device structures,[1d,8a,9b,13,21] suggesting that it is a common LEC phenomenon. Further support for that it is indeed the selection of the ion-transporter additive that is causing the difference in light-emission behavior is provided by the results for the TMPE-OH/OC-blend LEC in Figures S1,S3, Supporting Information. In short, this device behaves as an intermediate of the single ion-transporter TMPE-OH LEC and TMPE-OC LEC, with the steady state EZ positioned at an intermediate value of 0.44, the spectral shape being an effective average, and the turn-on kinetics being slower than the TMPE-OH LEC but faster than the TMPE-OC LEC.

We now attempt to shed light on the origin of the differing EZ behavior of our investigated LEC devices. To this end, we have performed the numerical drift-diffusion simulation displayed in **Figure 3**a. It reveals that the initial EZ position is

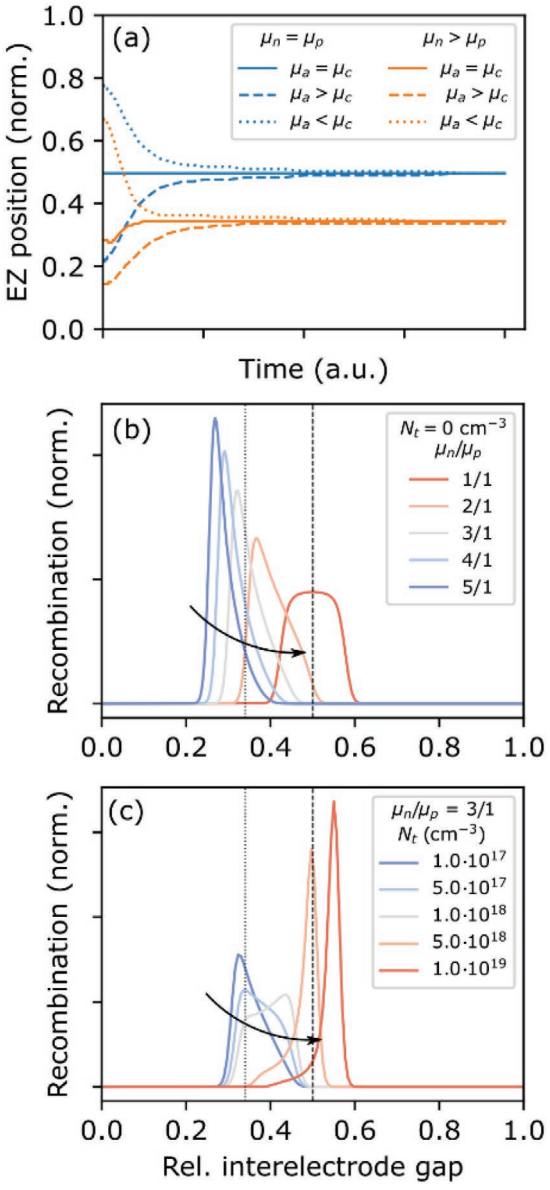

Figure 3. a) Simulated transients for the position of the emission zone in the active material for different values for the mobility of the electrons (μ_n), the holes (μ_p), the anions (μ_a), and the cations (μ_c), as identified in the inset. Simulated steady-state electron:hole recombination profiles for: b) a trap-free active material at different μ_n/μ_p ratio, as identified in the legend; c) an electron-trap-containing active material, with the trap-free electron and hole mobility ratio being $\mu_n/\mu_p = 3$, and with the electron trap density, N_t, defined in the inset.

decided by the ratio between the mobility of the anions (μ_a) and the mobility of the cations (μ_c), with a μ_a/μ_c ratio larger than 1 resulting in an initial EZ that forms closer to the anodic interface at 0; see the dashed lines in Figure 3a. This can be conceptually explained by that the higher-mobility (i.e., faster-drifting) negative anions initially accumulate at a high concentration in a small volume next to the positive anode, whereas the lower-mobility (i.e., slower) cations accumulate at a lower concentration in a larger volume at the cathode. This in turn enables a corresponding higher p-type doping (hole plus anion) concentration in the smaller volume next to the anode, and a lower n-type doping (electron plus cation) concentration in the larger volume at the cathode (remember that the total number of p-type and n-type dopants must be balanced in a symmetric LEC device for electroneutrality reasons[14,18]). For the opposite scenario, with the μ_a/μ_c ratio being smaller than 1, the initial EZ forms closer to the cathode (see dotted lines in Figure 3a).

The steady-state EZ position is, in contrast, dictated by the ratio between the mobility of the electrons (μ_n) and the mobility of the holes (μ_p), with a μ_n/μ_p ratio larger (smaller) than 1 resulting in that the steady-state EZ forms closer to the anode (cathode); compare orange lines with blue lines in Figure 3a. At this point in time, the ion mobility ratio has no influence on the EZ position. We mention that these simulation findings on the influence of the anion/cation mobility ratio and the electron/hole mobility ratio on the initial and the steady-state position of the EZ, respectively, are in agreement with the results presented in ref. [6b].

A comparison with the measured EZ transients in Figure 2a,b and Figure S2a–d, Supporting Information, (marked by crosses) reveal that the behavior of the TMPE-OH LEC is most reminiscent of the dotted blue line ($\mu_a < \mu_c$; $\mu_n = \mu_p$) in Figure 3a, while the TMPE-OC LEC performs similar to the dashed orange line ($\mu_a > \mu_c$; $\mu_n > \mu_p$). Thus, the conclusion as regards to ionic mobility is that the TMPE-OH LEC exhibits higher mobility for the K^+ cations than the $CF_3SO_3^-$ anions, while the situation is reversed for the TMPE-OC LEC for which the $CF_3SO_3^-$ anions exhibit the larger mobility. We further remember that the time to V_{min} and steady state was significantly shorter for the TMPE-OH LEC, which implies that its active material features higher total ionic mobility. The distinguishing TMPE based ion transporter is primarily solvating and transporting the K^+ cation, while the $CF_3SO_3^-$ anion is very weakly coordinated and essentially "free".[15a,b] Thus, a plausible explanation for the observed mobility behavior is that the anion mobility is essentially the same in both LECs, whereas the cation mobility is higher with the smaller TMPE-OH ion transporter than the larger TMPE-OC. However, we emphasize that other factors, such as the active-material morphology,[15a,22] the initial spatial distribution of the electrolyte,[21a] and the release kinetics of cations from the electrolyte complex,[23] also can influence the effective ion mobility. In the morphology context, we mention that an AFM study revealed that the active materials featured a very smooth surface morphology, regardless of the ion-transporter selection (see Figure S4, Supporting Information).

We find that the steady-state EZ position is also strongly influenced by the selection of the ion-transporter additive, with the steady-state EZ value being 0.48 for the TMPE-OH LEC, 0.44 for the TMPE-OH/OC-blend LEC, and 0.34 for the TMPE-OC LEC (see Figure S3, Supporting Information). This is particularly interesting and surprising since the simulation study in Figure 3a reveals that the steady-state position of the EZ is solely dictated by the electron and hole mobility of the OSC, and since the OSC is the same for both LECs (i.e., the conjugated polymer Super Yellow). More specifically, the comparison between the measured and simulated EZ transients provides that the TMPE-OH LEC features an approximately equal electron and hole mobility (because of the centered steady-state position of the EZ), whereas the electrons are significantly more mobile than the holes in the TMPE-OC LEC (with its steady-state EZ located closer to the anode).

Figure 3b presents a systematic drift-diffusion simulation study, which shows that a shift of the steady-state EZ position from 0.32 to 0.50 (similar to the observed change induced by changing from TMPE-OC to TMPE-OH) can be accomplished by decreasing the effective μ_n/μ_p ratio from 3 to 1 in a trap-free active material (as indicated by the arrow in Figure 3b). Alternatively, Figure 3c shows that a similar shift of the EZ position (in an active material with a trap-free μ_n/μ_p ratio of 3) can be achieved by introducing electron traps, with a trap depth of 0.30 eV, at a concentration of $N_t = 5 \times 10^{18}$ cm^{-3}. We mention that this particular concentration of "extrinsic" traps, as formed by the blending of Super Yellow with the TMPE-OH ion transporter, is one order of magnitude higher than the "intrinsic" trap concentration of pristine Super Yellow, as reported in, for example, ref. [24], but that the nominal concentration of TMPE-OH in the active material is even higher. Figure S5, Supporting Information, presents the associated ion and electron profiles at steady state for relevant mobility and trap scenarios. The shift of the μ_n/μ_p ratio from 3 to 1 in a trap-free material results in the expected attainment of symmetric (and coupled) electron and ion (i.e., doping) gradients and a symmetric EZ peak (compare Figure S5b, Supporting Information, with Figure S5a, Supporting Information), whereas the introduction of the electron traps results in a preferential and essentially complete filling of the electron traps and a concomitant lowering of the concentration of "free" electrons in the n-doping region (compare Figure S5b, Supporting Information, with Figure S5c,d, Supporting Information).

We have measured the influence of the two ion-transporter additives on the electronic transport properties of Super Yellow in hole-only and electron-only devices in Figure S6, Supporting Information. Note that the active material was free from ions in order to eliminate effects related to ion redistribution. We note in passing that our measurement on the pristine Super Yellow devices are in good agreement with the results reported by Niu and co-workers.[24] We find that the pristine Super Yellow and the Super Yellow:TMPE-OC blend exhibit similar values for the electron and hole currents, but that the addition of TMPE-OH to Super Yellow significantly lowers the current. We emphasize that these data were recorded at much lower charge carrier concentration than in effect in the doping regions of an LEC (because of the charge-screening role of the mobile ions), and that it is therefore advisable to not draw quantitative conclusions as regards to the anticipated EZ position in an LEC device

from these data. Nevertheless, it appears as though the addition of the TMPE-OC ion transporter essentially leaves the transport properties of Super Yellow intact, whereas the addition of the smaller, more polar, hydrogen-bonding TMPE-OH ion transporter lowers the transport capacity of Super Yellow. We speculate that such specific TMPE-OH:Super Yellow molecular interactions could originate in TMPE-OH induced charge-trapping and/or hydrogen-bonding interactions, and hope to be able to shed light on this intriguing issue in a future publication.

We finally attempt to establish the primary mechanism for why the shift of the EZ position, as induced by the change of ion-transporter additive, results in the observed strong changes in the light-emission performance. For this exercise, we call attention to that the EZ position in the active material can influence the emission performance of LEC (and OLED) devices by (at least) three different mechanisms: i) cavity effects,[4c,9b,16,25] ii) exciton quenching by nearby metal electrodes,[26] and iii) exciton quenching by nearby dopants (or polarons).[4c]

Figure 1b illustrates the origin of the cavity effect. The photons that are generated by the radiative decay of excitons (which in turn are formed by electron and hole recombination) in the EZ can either travel directly toward the transparent (ITO) electrode and be outcoupled, or alternatively travel toward the reflective (Al) electrode, be reflected, and thereafter be outcoupled at the ITO. If the optical path difference between the directly outcoupled photon beam and the reflected photon beam ($\Gamma = 2nd\cos\beta$, where n is the refractive index of the active material, d the distance between the EZ and the reflective electrode, and β the angle between the photon beam and the normal of the reflective electrode) is an odd (even) multiple of half the photon wavelength, then the two photon beams will cancel each other (add up) by destructive (constructive) interference. The exciton quenching by nearby metal electrodes and dopants instead originates in energy-transfer and/or charge-transfer reactions, which are sensitively dependent on the distance between the excitons (in the EZ) and the metals and the dopants.

The dashed lines in Figure 2a,b and Figure S2a–d, Supporting Information, present a simulation of the forward luminance, which uses the measured EZ position as the "free parameter" input and which considers losses because of the cavity effect and the exciton-electrode quenching, but not the exciton-dopant quenching. The simulated peak luminance was normalized to the measured peak luminance, which implies that the simulation solely captures the relative change in the luminance by a moving EZ position. Nevertheless, the consistent excellent agreement between simulation and experiment suggests that the losses to exciton-doping quenching are relatively constant during these experiments. However, we emphasize that the losses to exciton-doping quenching are still expected to be significant in this single-OSC LEC, as convincingly demonstrated in ref. [4b], but that it appears as though the magnitude of this loss is relatively invariant toward the observed EZ shift. Moreover, since the measured EZ in the herein presented experiments is invariably at least 30 nm away from an electrode interface (see Figure S3a, Supporting Information), it is reasonable that the exciton-electrode quenching is comparatively minor, and that the observed changes in the light-emission performance are primarily due to a changing cavity condition.

3. Conclusion

We report that the light-emission performance of a common LEC device can be significantly and practically improved by the inclusion of an appropriate additive into the active material. We establish that a key role of such a functional additive is to alter the electron and hole mobility ratio of the OSC so that the steady-state EZ is shifted to a favorable position in the active material for suppressed destructive interference. The merit of the approach is exemplified through the employment of two different star-branched oligomer additives, which are solely distinguished by that their end-capping unit is either polar, hydrogen bonding, and short or more hydrophobic and extended. We demonstrate that a shift from the latter to the former results in a balancing of the hole and electron mobility on the OSC and a centering of the steady-state EZ position, which is manifested in a 60% increase in the power efficiency and an angle-independent luminance. The important take-home message from our study is thus that it is possible to efficiently shift the EZ position for an improved LEC performance by the straightforward inclusion of an easily modified and low-cost additive in the active material.

4. Experimental Section

Device Fabrication: Figure 1a presents the chemical structure of the constituents in the active material. The EL OSC was a phenyl-substituted poly(paraphenylene vinylene) conjugated copolymer termed "Super Yellow" (Merck, Darmstadt, DE), the salt was KCF_3SO_3 (Sigma Aldrich, USA), and the ion transporter was TMPE, which was end-capped with either hydroxyls (TMPE-OH, M_n = 450 g mol^{-1}, Sigma Aldrich, USA) or n-octyl carbonates (TMPE-OC, M_n = 918 g mol^{-1}). The synthesis of TMPE-OC is described in ref. [15a]. The salt and the ion transporters were dried in a vacuum oven at 150 °C and 50 °C, respectively, for 12 h before the preparation of inks, while Super Yellow was used as received. The active-material constituents were separately dissolved in in cyclohexanone (Sigma Aldrich, USA) in the following concentrations: KCF_3SO_3 and TMPE-OH/TMPE-OC: 10 g L^{-1}; Super Yellow: 10–15 g L^{-1}; the higher Super Yellow concentration resulted in a thicker active-material film. The active-material ink was prepared by mixing these master inks in a solute mass ratio of Super Yellow:TMPE-OH:KCF_3SO_3 = 1:0.15:0.03, Super Yellow:TMPE-OC:KCF_3SO_3 = 1:0.20:0.03, or Super Yellow:TMPE-OH:TMPE-OC:KCF_3SO_3 = 1:0.075:0.075:0.03. In this context, the authors mention that a higher mass fraction for TMPE-OC resulted in severe phase separation in the dry active-material film. The authors also mention that they found that a long-term storage (>2 years) of TMPE-OC resulted in a sub-par device performance and that they therefore only employed short-term stored (<1 year) TMPE-OC in this study.

Figure 1b presents a schematic of the LEC device structure. The transparent indium-tin-oxide (ITO) coated glass substrate (145 nm, R_s = 20 Ω □$^{-1}$, thin film devices) was cleaned by sequential ultrasonic treatment in detergent (Extran MA 01, Merck), deionized water, acetone, and isopropanol. The active-material ink was spin-coated on the ITO for 60 s, and thereafter dried at 70 °C for at least 2 h. The dry thickness of the active material (d_{AM}) was controlled by the spin speed (1000–4000 rpm) and the Super Yellow concentration, and measured with a stylus profilometer (DektakXT, Bruker). The reflective Al top electrode (thickness = 100 nm) was deposited by thermal evaporation under vacuum ($p < 8 \times 10^{-6}$ mbar) through a shadow mask. The overlap of the transparent ITO anode and the reflective Al cathode defined four independent 2 × 2 mm^2 LEC devices on each substrate. The LECs were finally protected from the ambient air by attaching a thin glass lid on top of the Al cathodes, using either a UV-curable epoxy (Ossila) for the

TMPE-OH LEC or a flexible pressure-sensitive adhesive for the TMPE-OC LEC; see ref. [27] for more details on the encapsulation procedure.

The hole-only devices featured an ITO/PEDOT:PSS/active-material/Au architecture. The device fabrication was identical to that of the LEC, with the notable exceptions that the ITO anode was spin-coated with a thin layer of PEDOT:PSS (dry thickness = 20 nm, Clevios P VP AI 4083, Heraeus) following a 10 min exposure of the ITO surface to UV-ozone (model 42–220, Jelight Company), that the active material was free from the KCF_3SO_3 salt, and that the top cathode was Au. The Al/active-material/Ca electron-only devices were also free from salt in the active material, but comprised thermally evaporated Al as the bottom anode and thermally evaporated Ca as the top cathode. Only data for devices with $d_{AM} \geq 100$ nm were reported, since thinner devices suffered from a significant device-to-device variation, presumably due to short circuits or a local thinning of the active material.

Device Characterization: The LEC devices were driven by a constant current density of 25 mA cm^{-2}, with the compliance voltage set to 21 V, and with ITO biased as the positive anode. A source-measure unit (Keithley 2400) supplied the current and recorded the corresponding voltage. An Al heat sink was placed behind the LEC device to mitigate undesired self-heating effects during electrical driving.[28] The angle-resolved EL intensity and spectrum of the LEC devices were measured with a custom-built, automated spectrogoniometer setup, as schematically depicted in Figure 1c. The device under study was placed in a connection jig, which aligned the emission area of the device with the rotation axis of a stepper motor. This rotation defined the viewing angle of the device, with 0° corresponding to the forward emission. The viewing angle was varied between −80° to 80° in steps of 5° or 10°, and controlled with a Python-based virtual instrument. A fraction of the device emission was collected by a collimating lens (∅ = 7.2 mm, F230 SMA-A, Thorlabs, Germany) positioned 75 mm away from the device, resulting in a small and constant solid collection angle (Ω) of 0.007 sr. An optical fiber delivered the collected light to a CCD-array spectrometer (Flame-S, OceanOptics). More details on the measurement setup and procedure can be found in ref. [16]. The current–voltage characterization of the non-encapsulated hole-only and electron-only devices was performed in a N_2-filled glove box (O_2 and water content < 1 ppm).

Optical Modeling and Fitting: The optical simulation was performed with the commercial software Setfos (version 5.1, Fluxim AG, Switzerland) on the device stack displayed in Figure 1b, that is, a glass substrate (thickness: 0.75 mm), an ITO anode (145 nm), an active material (the thickness was varied in the simulation), and an Al cathode (100 nm). The optical properties of the active material was set equal to those of undoped Super Yellow. The active material was divided into three layers: a 10-nm transparent layer sandwiched between two absorbing layers. The emitting dipoles, that is, the EZ, were represented by a delta distribution of isotropic dipoles positioned in the center of the transparent layer, and their intrinsic emission spectrum was set equal to the measured photoluminescence (PL) spectrum of a 17-nm thin film of Super Yellow. Figure S7, Supporting Information, shows that the PL spectrum of thicker (≥30 nm) Super Yellow films featured obscuring cavity effects. The simulation delivered the luminance and the emission spectrum as a function of the viewing angle as well as the EZ position.

The position of the EZ within the active material was derived by minimizing the root mean square error between the measured and the simulated data (Δ_{sim}^{meas}) for a set of wavelengths and viewing angles as:

$$\Delta_{sim}^{meas}(EZ) = \left(\frac{1}{N_\theta} \sum_\theta \frac{1}{N_\lambda} \sum_\lambda \left[I_{\theta,\lambda}^{meas} - I_{\theta,\lambda}^{sim}(EZ) \right]^2 \right)^{1/2} \quad (1)$$

with the only free fitting parameter being the selected value for the EZ position in the simulation and $I_{\theta,\lambda}$ is the spectral radiant intensity normalized to the $I_{0°,\lambda_{max}}$ value.

The speed of the fitting was improved by the concept of error landscape. In short, a set of solutions for $I_{\theta,\lambda}^{sim}(EZ)$ for each measured value of d_{AM} was generated, with the EZ varying between 0.05 and 0.95 in 0.01 steps. Figure S8, Supporting Information, visualizes the values for Δ_{sim}^{meas} in color-coded format for the determination of the EZ position as a function of time, with a yellow color identifying the best fit. It was found that the fitting of the position of the EZ resulted in essentially the same value, regardless of whether the entire active material was assigned with the complex refractive index of the pristine active material or whether the doping-induced changes of the refractive index were considered. This finding was in agreement with ref. [4c]. The peak value for the simulated luminance (dashed lines in Figure 2a,b and Figure S2a–d, Supporting Information) was normalized to that of the peak value of the measured luminance.

Drift-Diffusion Modeling: The numerical drift-diffusion simulation was performed with the drift-diffusion module of Setfos, which utilized the implicit Euler method to solve the continuity, the drift-diffusion, and the Poisson equations. Since Setfos was not capable of capturing the modification of the interfacial electric field following the EDL formation, it was compensated by setting the injection barriers at the cathodic and anodic interface to a small and equal value of 0.1 eV. The general selection of the model parameters was inspired by ref. [21a], and is listed in Table S2, Supporting Information. The simulated devices were driven by a constant voltage of 3.5 V. The total transient simulation time was 100 ms, with a logarithmic time step of 50 steps per decade. A relative change of the charge carrier distribution of $< 1 \times 10^{-10}$ was the convergence criterion for a time step. We elected to only present transient data for times >250 µs, since Setfos did not capture the EDL formation.

Supporting Information

Supporting Information is available from the Wiley Online Library or from the author.

Acknowledgements

The authors gratefully acknowledge Andreas Poehlmann for the development of the open-source python-seabreeze library for the control of the Ocean Optics spectrometer, and Mikael Fredriksson at Umeå University for his contribution to the 3D printing of the spectrogoniometer setup. The authors also gratefully acknowledge the reviewers for their constructive input, which helped them improve the clarity and quality of the manuscript. The authors finally acknowledge generous financial support from Kempestiftelserna, the Swedish Research Council, the Swedish Energy Agency, the Swedish Foundation for Strategic Research, Stiftelsen Olle Engkvist Byggmästare, Wenner-Gren Foundations, and Bertil and Britt Svenssons stiftelse för belysningsteknik.

Conflict of Interest

The authors declare no conflict of interest.

Data Availability Statement

The data that support the findings of this study are available from the corresponding author upon reasonable request.

Keywords

electron mobility, emission zone position, light-emission efficiency, light-emitting electrochemical cell, microcavity effect, tunable additive

Received: September 30, 2021
Revised: December 7, 2021
Published online: January 15, 2022

[1] a) L. Edman, *Electrochim. Acta* **2005**, *50*, 3878; b) Q. B. Pei, G. Yu, C. Zhang, Y. Yang, A. J. Heeger, *Science* **1995**, *269*, 1086; c) J. Gao, *Curr. Opin. Electrochem.* **2018**, *7*, 87; d) A. Jiménez-Solano, L. Martínez-Sarti, A. Pertegás, G. Lozano, H. J. Bolink, H. Míguez, *Phys. Chem. Chem. Phys.* **2020**, *22*, 92; e) J. E. Namanga, N. Gerlitzki, A.-V. Mudring, *Adv. Funct. Mater.* **2017**, *27*, 1605588; f) A. Puthanveedu, K. Shanmugasundaram, S. Yoon, Y. Choe, *J. Mater. Chem. C* **2021**, *9*, 8265; g) K. Schlingman, Y. T. Chen, R. S. Carmichael, T. B. Carmichael, *Adv. Mater.* **2021**, *33*, 2006863.

[2] a) A. C. , D. K. Dubey, M. Pahlevani, G. C. Welch, *Adv. Mater. Technol.* **2021**, *6*, 2100264; b) J. H. Burroughes, D. D. C. Bradley, A. R. Brown, R. N. Marks, K. Mackay, R. H. Friend, P. L. Burns, A. B. Holmes, *Nature* **1990**, *347*, 539; c) C. W. Tang, S. A. Vanslyke, *Appl. Phys. Lett.* **1987**, *51*, 913; d) C. Keum, C. Murawski, E. Archer, S. Kwon, A. Mischok, M. C. Gather, *Nat. Commun.* **2020**, *11*, 11.

[3] a) R. Meerheim, M. Furno, S. Hofmann, B. Lüssem, K. Leo, *Appl. Phys. Lett.* **2010**, *97*, 253305; b) W. Brütting, J. Frischeisen, T. D. Schmidt, B. J. Scholz, C. Mayr, *Phys. Status Solidi A* **2013**, *210*, 44.

[4] a) S. van Reenen, M. V. Vitorino, S. C. J. Meskers, R. A. J. Janssen, M. Kemerink, *Phys. Rev. B* **2014**, *89*, 205206; b) S. van Reenen, R. A. J. Janssen, M. Kemerink, *Adv. Funct. Mater.* **2015**, *25*, 3066; c) E. M. Lindh, P. Lundberg, T. Lanz, L. Edman, *Sci. Rep.* **2019**, *9*, 10433; d) J. Ràfols-Ribé, E. Gracia-Espino, S. Jenatsch, P. Lundberg, A. Sandström, S. Tang, C. Larsen, L. Edman, *Adv. Opt. Mater.* **2020**, *9*, 2001405; e) T. Lanz, E. M. Lindh, L. Edman, *J. Mater. Chem. C* **2017**, *5*, 4706.

[5] a) S. L. M. van Mensfoort, M. Carvelli, M. Megens, D. Wehenkel, M. Bartyzel, H. Greiner, R. A. J. Janssen, R. Coehoorn, *Nat. Photonics* **2010**, *4*, 329; b) S. R. Forrest, *Nature* **2004**, *428*, 911.

[6] a) P. Matyba, K. Maturova, M. Kemerink, N. D. Robinson, L. Edman, *Nat. Mater.* **2009**, *8*, 672; b) S. van Reenen, P. Matyba, A. Dzwilewski, R. A. Janssen, L. Edman, M. Kemerink, *J. Am. Chem. Soc.* **2010**, *132*, 13776.

[7] a) A. Sandström, L. Edman, *Energy Technol.* **2015**, *3*, 329; b) Z. Shu, F. Kemper, E. Beckert, R. Eberhardt, A. Tunnermann, *Mater. Today: Proc.* **2017**, *4*, 5039; c) Z. T. Zhang, K. P. Guo, Y. M. Li, X. Y. Li, G. Z. Guan, H. P. Li, Y. F. Luo, F. Y. Zhao, Q. Zhang, B. Wei, Q. B. Pei, H. S. Peng, *Nat. Photonics* **2015**, *9*, 233; d) J. J. Liang, L. Li, X. F. Niu, Z. B. Yu, Q. B. Pei, *J. Phys. Chem. C* **2013**, *117*, 16632; e) J. M. Leger, *Adv. Mater.* **2008**, *20*, 837.

[8] a) S. Jenatsch, M. Regnat, R. Hany, M. Diethelm, F. Nuesch, B. Ruhstaller, *ACS Photonics* **2018**, *5*, 1591; b) M. Diethelm, A. Schiller, M. Kawecki, A. Devižis, B. Blülle, S. Jenatsch, E. Knapp, Q. Grossmann, B. Ruhstaller, F. Nüesch, R. Hany, *Adv. Funct. Mater.* **2020**, *30*, 1906803.

[9] a) S. Tang, A. Sandström, P. Lundberg, T. Lanz, C. Larsen, S. van Reenen, M. Kemerink, L. Edman, *Nat. Commun.* **2017**, *8*, 1190; b) T. W. Wang, H. C. Su, *Org. Electron.* **2013**, *14*, 2269.

[10] a) C. L. Lee, C. Y. Cheng, H. C. Su, *Org. Electron.* **2014**, *15*, 711; b) J. Wang, S. Tang, A. Sandström, L. Edman, *ACS Appl. Mater. Interfaces* **2015**, *7*, 2784.

[11] Y. F. Hu, J. Gao, *Appl. Phys. Lett.* **2006**, *89*, 253514.

[12] J. H. Shin, N. D. Robinson, S. Xiao, L. Edman, *Adv. Funct. Mater.* **2007**, *17*, 1807.

[13] R. Sun, C.-T. Liao, H.-C. Su, *Org. Electron.* **2014**, *15*, 2885.

[14] J. F. Fang, Y. L. Yang, L. Edman, *Appl. Phys. Lett.* **2008**, *93*, 3.

[15] a) J. Mindemark, S. Tang, J. Wang, N. Kaihovirta, D. Brandell, L. Edman, *Chem. Mater.* **2016**, *28*, 2618; b) S. Tang, J. Mindemark, C. M. G. Araujo, D. Brandell, L. Edman, *Chem. Mater.* **2014**, *26*, 5083; c) M. Diethelm, Q. Grossmann, A. Schiller, E. Knapp, S. Jenatsch, M. Kawecki, F. Nüesch, R. Hany, *Adv. Opt. Mater.* **2019**, *7*, 1801278.

[16] E. M. Lindh, P. Lundberg, T. Lanz, J. Mindemark, L. Edman, *Sci. Rep.* **2018**, *8*, 6970.

[17] S. van Reenen, T. Akatsuka, D. Tordera, M. Kemerink, H. J. Bolink, *J. Am. Chem. Soc.* **2013**, *135*, 886.

[18] J. Fang, P. Matyba, L. Edman, *Adv. Funct. Mater.* **2009**, *19*, 2671.

[19] S. van Reenen, P. Matyba, A. Dzwilewski, R. A. J. Janssen, L. Edman, M. Kemerink, *J. Am. Chem. Soc.* **2010**, *132*, 13776.

[20] E. Archer, S. Hillebrandt, C. Keum, C. Murawski, J. Murawski, F. Tenopala-Carmona, M. C. Gather, *Adv. Opt. Mater.* **2020**, *9*, 2000838.

[21] a) M. Diethelm, A. Schiller, M. Kawecki, A. Devižis, B. Blülle, S. Jenatsch, E. Knapp, Q. Grossmann, B. Ruhstaller, F. Nüesch, R. Hany, *Adv. Funct. Mater.* **2019**, *30*, 1906803; b) H. C. Su, *ChemPlusChem* **2018**, *83*, 197.

[22] a) F. P. Wenzl, P. Pachler, C. Suess, A. Haase, E. J. W. List, P. Poelt, D. Somitsch, P. Knoll, U. Scherf, G. Leising, *Adv. Funct. Mater.* **2004**, *14*, 441; b) Y. Cao, G. Yu, A. J. Heeger, C. Y. Yang, *Appl. Phys. Lett.* **1996**, *68*, 3218.

[23] I. Gerz, E. M. Lindh, P. Thordarson, L. Edman, J. Kullgren, J. Mindemark, *ACS Appl. Mater. Interfaces* **2019**, *11*, 40372.

[24] Q. Niu, G.-J. A. H. Wetzelaer, P. W. M. Blom, N. I. Crăciun, *Adv. Electron. Mater.* **2016**, *2*, 1600103.

[25] G.-R. Lin, H.-F. Chen, H.-C. Shih, J.-H. Hsu, Y. Chang, C.-H. Chiu, C.-Y. Cheng, Y.-S. Yeh, H.-C. Su, K.-T. Wong, *Phys. Chem. Chem. Phys.* **2015**, *17*, 6956.

[26] a) L. Penninck, S. Mladenowski, K. Neyts, *J. Opt.* **2010**, *12*, 075001; b) M. Furno, R. Meerheim, S. Hofmann, B. Lüssem, K. Leo, *Phys. Rev. B* **2012**, *85*, 115205.

[27] A. Asadpoordarvish, A. Sandström, S. Tang, J. Granström, L. Edman, *Appl. Phys. Lett.* **2012**, *100*, 193508.

[28] J. Ràfols-Ribé, N. D. Robinson, C. Larsen, S. Tang, M. Top, A. Sandström, L. Edman, *Adv. Funct. Mater.* **2020**, *30*, 1908649.